Journal of Nuclear Cardiology (2024) 39, 101911

ORIGINAL RESEARCH

Quantitative assessment of cardiac ^{123}iodo-metaiodobenzylguanidine SPECT/CT in patients with arrhythmogenic right ventricular cardiomyopathy: Novel insight in disease monitoring

Johannes M. Hagen [1], Mathias J. Zacherl, MD [1], Matthias Brendel, MD [1,4,5], Sebastian Clauß, MD [2,3,6,7,8], Stefan Kääb, MD [2,3,6,7,8], Peter Bartenstein, MD [1], Andrei Todica, MD [1], Guido Böning, PhD [1], Maximilian Fischer, MD [2,3,*]

[1] Department of Nuclear Medicine, Ludwig-Maximilians-University, Munich 81377, Germany
[2] Medizinische Klinik und Poliklinik I, Klinikum der Universität München, Ludwig-Maximilians-Universität, Marchioninistrasse 15, 81377 Munich, Germany
[3] DZHK (German Centre for Cardiovascular Research), Partner Site Munich Heart Alliance, Munich, Germany
[4] German Center for Neurodegenerative Diseases (DZNE), Munich, Germany
[5] Munich Cluster for Systems Neurology (SyNergy), Munich, Germany
[6] Institute of Surgical Research at the Walter-Brendel-Center of Experimental Medicine, University Hospital, LMU Munich, Marchioninistrasse 27, D-81377 Munich, Germany
[7] Member of the European Reference Network for Rare, Low Prevalence and Complex Diseases of the Heart (ERN GUARD-Heart), the Netherlands
[8] Interfaculty Center for Endocrine and Cardiovascular Disease Network Modelling and Clinical Transfer (ICONLMU), LMU Munich, Munich, Germany

[*] Corresponding author. LMU University Hospital, LMU Munich, Department of Medicine I, Marchioninistraße 15, 81377 Munich, Germany.
E-mail address: Maximilian.Fischer@med.uni-muenchen.de (Maximilian Fischer).

Abstract

Background: The heart-to-mediastinum ratio (H/M-Ratio) of ^{123}iodo-metaiodo benzylguanidine (^{123}I-MIBG) represents state-of-the-art assessment for sympathetic dysfunction in patients with arrhythmogenic right ventricular cardiomyopathy (ARVC). This study aims to evaluate quantitative reconstruction of ^{123}I-MIBG uptake and to demonstrate its correlation with echocardiographic parameters.

Methods: Cardiac innervation was assessed in 23 patients diagnosed with definite ARVC or borderline ARVC and 12 patients with other cardiac disease presenting arrhythmia, using quantitative ^{123}I-MIBG Single Photon Emission Computed Tomography/Computed Tomography (SPECT/CT) imaging. Tracer uptake was evaluated in the left (LV) and right ventricle (RV) based on a CT scan after quantitative image reconstruction. The relationship between tracer uptake and echocardiographic parameter data was examined.

Results: Absolute quantification of ^{123}I-MIBG uptake in the LV and RV is feasible and correlates accurately with the gold standard H/M Ratio. When comparing sensitivity and specificity, the area under the curve (AUC) favors standardized uptake value (SUV) of the RV over the right-ventricle-to-mediastinum-ratio (RV/M-Ratio) for diagnosing ARVC. A reduced RV-SUV in patients with definite ARVC is associated with reduced RV function. RV polar maps revealed globally reduced ^{123}I-MIBG uptake without segment-specific reduction in the RV.

Conclusions: Quantitative ^{123}I-MIBG SPECT in ARCV patients offers robust potential for clinical reporting and demonstrates a significant correlation with RV function. Segmental RV analysis needs to be evaluated in larger samples. In summary, cardiac

Received 27 March 2024; Accepted 3 July 2024; Available online 14 July 2024

https://doi.org/10.1016/j.nuclcard.2024.101911

^{123}I-MIBG imaging using SUV could facilitate image-guided therapy in patients diagnosed with ARVC.

Keywords: ARVC, MIBG, Heart-to-mediastinum-ratio, SUV, SPECT/CT

ABBREVIATIONS

ARVC	arrhythmogenic right ventricular cardiomyopathy
H/M-Ratio	heart-to-mediastinum-ratio
^{123}I-MIBG	^{123}iodo-metaiodobenzylguanidine
LV/M-Ratio	left-ventricle-to-mediastinum-ratio
LV-SUV	standardized uptake value of the left ventricle
RV/M-Ratio	right-ventricle-to-mediastinum-ratio
RV-SUV	standardized uptake value of the right ventricle
SPECT/CT	Single Photon Emission Computed Tomography/ Computed Tomography
SUV	standardized uptake value
VOI	volume of interest

INTRODUCTION

Arrhythmogenic right ventricular cardiomyopathy (ARVC) is classified among the primary cardiomyopathies [1]. It typically presents in individuals aged 10 to 40 years. The disease more frequently affects men than women. As the disease progresses, patients may develop electrical instability leading to cardiac arrhythmias and heart failure. Sudden cardiac death can be an initial symptom. Other manifestations include palpitations, arrhythmias, syncope, and heart failure, which may necessitate heart transplantation at a young age (mean age 38.7 $\pm$ 13.4 years at the time of first arrhythmia) [2–4]. The prognosis of ARVC is variable, with annual mortality reported between .08% and 4% [5–7].

Genetically determined dysfunction of cell-cell contacts is hypothesized to initiate cardiomyocyte pathology, which forms the basis of the disease. Consequently, affected areas undergo replacement with connective tissue. The compromised cellular architecture, compounded by mechanical stress, leads to morphological alterations, including ventricular dilatation. This process begins in the right ventricle (RV) and extends to the left ventricle (LV) in approximately three-quarters of patients [1,2,8–12]. Cardiac arrhythmias are believed to arise due to the impairment and subsequent decline of the sympathetic nervous system in the heart [13–15]. Programmed cell death (apoptosis) is a proposed mechanism for ARVC pathology [16], which might lead to cardiac electrical remodeling (e.g. re-entry mechanism) and thus makes ARVC hearts prone to cardiac arrhythmia [2,9]. The cardiac remodeling might contribute to arrhythmia besides the known autonomic dysfunction.

Nuclear medicine examination of the sympathetic nervous system with ^{123}iodo-metaiodobenzylguanidine (^{123}I-MIBG) has revealed decreased tracer uptake in patients with ARVC. Single Photon Emission Computed Tomography/ Computed Tomography (SPECT/CT) imaging enabled the separate assessment of tracer uptake in both ventricles [17,18].

Previous studies determined ^{123}I-MIBG-tracer uptake using the heart-to-mediastinum-ratio (H/M-Ratio) without obtaining absolute values [18–21]. The standardized uptake value (SUV) has long been calculated for positron-emission-tomography (PET) [22] and recent research suggested that SUV can be a valuable quantitative parameter for SPECT/CT imaging [23–28]. We hypothesized the feasibility of determining cardiac SUV separately in the LV and RV and aimed:

(I) Investigated whether the SUVs of the LV and RV correlate with the ratios to the mediastinum (LV/M-Ratio, RV/M-Ratio).
(II) Compare the SUVs of patients with various diagnoses.
(III) Assess the SUVs of both ventricles against functional echocardiography parameters and evaluate the use of RV polar maps to identify tracer uptake patterns.

METHODS

Study cohort

We retrospectively analyzed patients who underwent cardiac ^{123}I-MIBG scintigraphy from 2010 to 2022 at the Department of Nuclear Medicine, LMU University Hospital, LMU Munich. Patients underwent cardiac ^{123}I-MIBG-imaging either as part of previous clinical studies or as diagnostic

evaluation of cardiac innervation by the referring cardiology department. To focus on patients with primary arrhythmogenic disorders, we excluded those suffering from dilated cardiomyopathy and laminopathy. Additionally, one patient was excluded due to having undergone a heart transplantation. In a few instances, establishing a diagnosis from patient files was not feasible or there were missing data (including parameters such as size, weight, injected activity, or image data) (Figure 1).

For this study, we obtained the consent of the local ethics committee (project number: 22-0328). All individuals provided informed consent.

SPECT/CT imaging

SPECT image acquisition was performed according to a standardized protocol [18]. Image acquisition occurred 25 minutes (early) and 4 hours (delayed) after tracer injection. An average ^{123}I-MIBG-activity of 359.48 ± 41.79 MBq was administered. SPECT/CT was acquired using low energy, high-resolution collimator (matrix 64 x 64, pixel spacing 6.59, energy window 159 keV, width 15%, zoom factor 1.46, scan arc 90°, type of motion: step and shoot, frame duration 30 seconds, number of frames 32). Additionally, a low-dose CT scan (130 kV, 20 mAs) was conducted. All scans were performed with a Symbia True-Point SPECT/CT scanner (Siemens Medical Systems, Erlangen, Germany).

Image analysis and interpretation

Image reconstruction was performed using Hybrid Recon Software (Hermes Medical Solutions, Stockholm, Sweden). Image analysis was

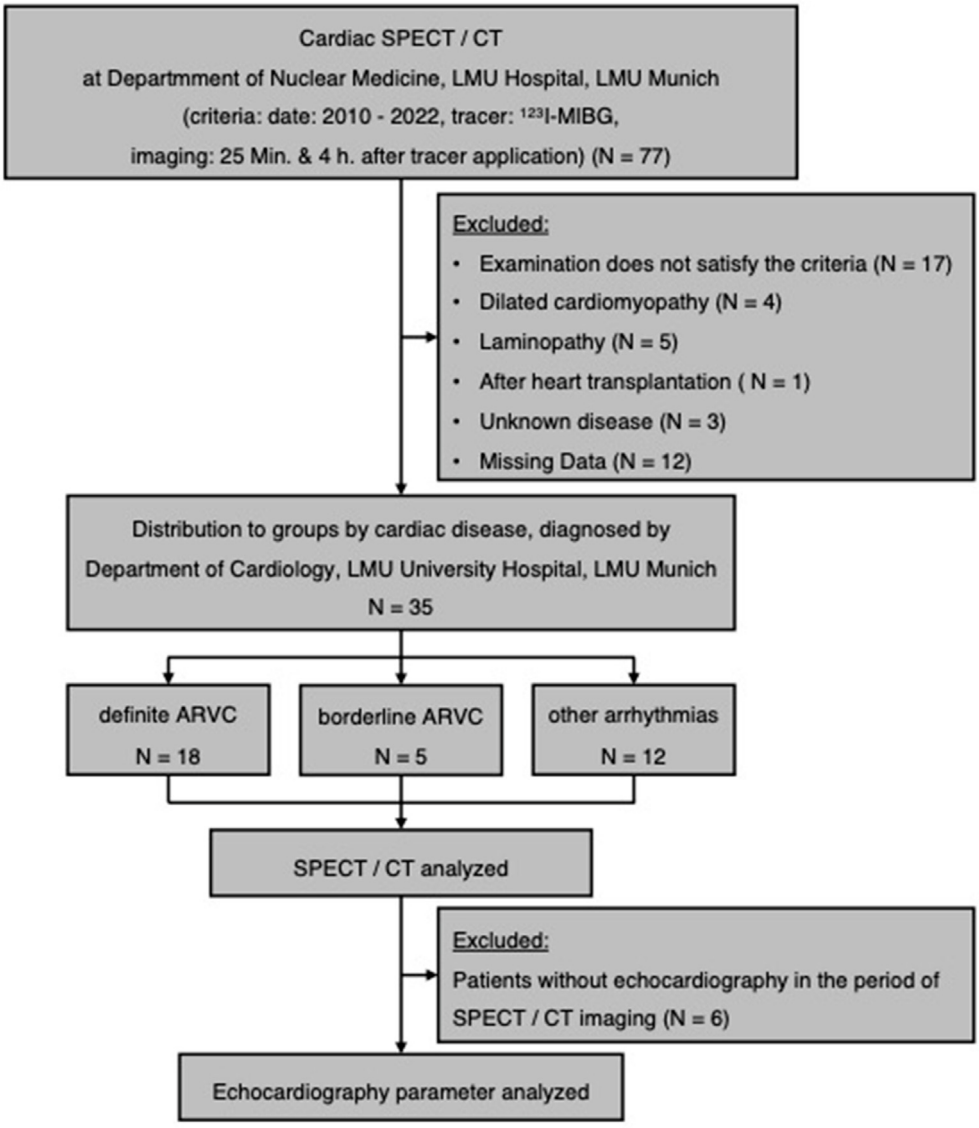

Figure 1. Patient selection and study process.

completed using PCARD (PMOD Technologies LL, Fälland, Swiss, Version 4.204). Using the SUV Image Calculation tool, image settings were adjusted to SUV, this required the input of the injected dose of ^{123}I-MIBG, time of injection as well as patient's height and weight. Subsequently, the CT image was fused with the SPECT image.

Following this, LV and RV short-axis images were manually reconstructed, resulting in images of vertical long-axis (VLA), horizontal long-axis (HLA), and short-axis (SA), corresponding to the LV or RV. After reorientation, a volume of interest (VOI) was delineated across all slices of the LV in images oriented to the LV-axis, and across all slices of the RV in images oriented to the RV-axis. The LV was detected automatically by the PMOD software, while the RV was detected manually by identifying the truncus pulmonalis in the CT image and following the right ventricular outflow tract caudally. Only the myocardium was included. The septum was attributed to the LV (Figure 2). The median SUV of the VOIs (LV-SUV, RV-SUV) and the median SUV of a cube in the mediastinum (33 mm edge length) were measured. The H/M-Ratio was calculated from the median ventricles' SUV and SUV of the mediastinal cube (LV-SUV for LV/M-Ratio and RV-SUV for RV/M-Ratio). Additionally, a polar map of LV and RV was created following the recommendations of American Heart Association (AHA) [29]. For the polar map of RV, only segments 1, 2, 3, 7, 8, 9, 13, 14 of polar plot were considered (Supplemental Figure 1) [30].

Diseases and echocardiography

Diagnoses were derived from the patient files of the Department of Cardiology, LMU University Hospital, LMU Munich. Diagnosis of ARVC is established using the modified task force criteria, which include findings from echocardiography, magnetic resonance imaging (MRI), histology electrocardiography, and patients' history; these are organized into major and minor categories. Classification into definite ARVC (2 major or 1 major and 2 minor criteria or 4 minor criteria from different categories), borderline ARVC (1 major and 1 minor or 3 minor criteria from different categories), or possible ARVC (1 major or 2 minor criteria from different categories) is determined by these findings [31]. Details on arrhythmias were gathered from the implantable cardioverter defibrillators (ICD) examinations and patient records. Echocardiographic data were subsequently evaluated based on ESC recommendations [32].

Statistical analysis

For statistical analysis, RStudio (Version 2023.06.0 + 421) was utilized.

Categorical or binary variables were expressed in absolute and relative frequencies. Metric variables were presented with their mean and standard deviation (SD). The data was tested for normal distribution using the Kolmogorov-Smirnov-Test. An Analysis of Variance (ANOVA) or Fisher's Exact Test was performed to compare more than two disease groups. If there was insufficient agreement among different groups, the t-test was used for a more detailed analysis. The Bonferroni method was employed to adjust the significance level. For correlation analyses, the Pearson correlation coefficient and test according to Pearson were conducted. The Bland-Altman-Plot was utilized to compare the two diagnostic methods. The intra- and interrater

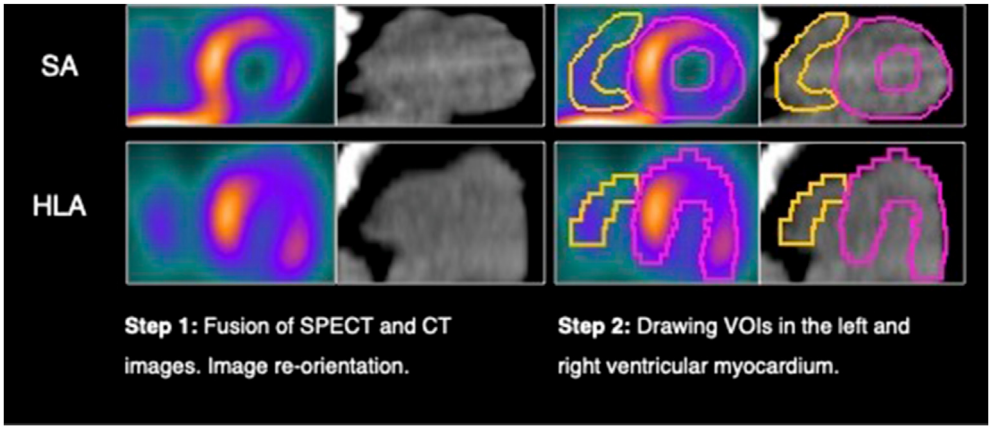

Figure 2. Image processing. The figure presents a delayed image of a patient diagnosed with ARVC.

reliability was assessed using Cohen's kappa. A generalized linear model, receiver operating characteristic (ROC) curves, and area under the curve (AUC) were calculated to present sensitivity and specificity. To compare the AUCs, Delong's test was used. The level of significance was set at .05.

RESULTS

Patient characteristics

^{123}I-MIBG scintigraphy was performed on patients with various cardiac diseases. The division of sex, age, administered ^{123}I-MIBG dose, and physical constitution of the patients was similar across all groups (Table 1).

Assessment of SUV in left and right ventricle compared to H/M-Ratio

SUV values of the ventricles were compared with respect to the diagnosed diseases (Figure 3). In delayed images, there was a significantly lower RV-SUV between the groups of definite ARVC (3.74 ± .31) and other arrhythmias (4.88 ± .59; $P < .001$). A similar investigation conducted on early images produced comparable results (Supplemental Figure 2): there was a significant difference between the group of definite ARVC (3.54 ± .74) and other arrhythmias (4.88 ± .59; $P < .001$). For the LV-SUV there was no significant difference.

The ventricles' SUVs were correlated with the ratio of ventricle-to-mediastinum-ratios and a Bland-Altman-Plot was created to compare the two methods. There was a significant correlation between RV-SUV and RV/M-Ratio (early images: $r = .61$, $P < .001$, Supplemental Figure 3; delayed images: $r = .78$, $P < .001$, Figure 4). The correlation between LV-SUV and LV/M-Ratio in early images was not significant ($r = .29$, $P = .089$; Supplemental Figure 4), but in delayed images, the correlation was significant ($r = .69$, $P < .001$; Figure 5). The Bland-Altman-Plot showed a good agreement with a certain variability for LV (early images: bias: - 3.81, Supplemental Figure 4; delayed images: bias: - 2.16, Figure 5) and RV (early images: bias: - 2.34, Supplemental Figure 3; delayed images: bias: - 1.37, Figure 4). The intra-rater reliability for RV-SUV was almost perfect (.86) and the interrater reliability was substantial (.71) underlining the methodical reproducibility.

A ROC was generated to investigate the SUV's diagnostic value for definite ARVC, and the AUC was calculated. The diagnosis of definite ARVC using SUV in terms of sensitivity and specificity when assessing the RV was more evident than when assessing the LV. The differences were significant for early images: AUC LV-SUV compared to AUC RV-SUV; $P < .05$ and for delayed images: AUC LV-SUV compared to AUC RV-SUV; $P < .05$. A comparison of AUC of SUV and the respective H/M-Ratio showed a difference in favor of SUV for both RV and LV (Figure 6).

Echocardiography

For the majority of patients (N = 29), echocardiography images were available for the period of scintigraphy (Table 2). These values were correlated to investigate the relationship between the SUV and functional echocardiography parameters. The correlation of LV-SUV and left ventricle ejection fraction (LV-EF) was significant in early images ($r = .43$, $P < .05$; Figure 7), but insignificant in delayed images ($r = .24$; $P = .2$; Supplemental Figure 5). However, there was a significant correlation between RV-SUV and measured fractional area change (FAC; early images: $r = .76$, $P < .001$, Fig 7; delayed images: $r = .73$, $P < .001$, Supplemental Figure 5) and between RV-SUV and tricuspid annular plane systolic excursion (TAPSE; early images: $r = .65$, $P < .001$, Figure 7; delayed images: $r = .68$, $P < .001$, Supplemental Figure 5).

Polar map

To determine regional innervation alterations, the segments of the LV and RV in the definite ARVC group were compared with the SUV of the respective ventricle. Consequently, the mean of the median LV-SUVs (early images: 6.45 ± 1.17, delayed images: 4.9 ± 1.27) and the median RV-SUVs (early images: 3.54 ± .74, delayed images: 2.71 ± .78) were calculated for the definite ARVC group. In early images, LV segment 8 (9.76 ± 1.99, $P < .001$), LV segment 9 (9.25 ± 2.07, $P < .01$), LV segment 10 (8.58 ± 1.77, $P < .05$), LV segment 12 (9.08 ± 2.09, $P < .05$) and LV segment 14 (8.96 ± 1.9, $P < .01$) were significantly different from the mean of median LV-SUVs. In delayed images, LV segment 8 (8.2 ± 2.59, $P < .05$) and LV segment 12 (7.19 ± 1.77, $P < .05$) were significantly different from the mean of median LV-SUVs. There was no significant difference in the RV (Figure 8).

DISCUSSION

The objective of this study was to examine the quantitative assessment of ^{123}I-MIBG SPECT in patients with ARVC and other arrhythmogenic diseases by imaging sympathetic dysfunction. For

Table 1. Baseline characteristics of the study population. Other Arrhythmias includes idiopathic ventricular fibrillation (IVFib), long-QT-Syndrom, catecholaminergic polymorphic ventricular tachycardia, neurocardiogenic syncope, Torsade-de-pointes-tachycardia, ventricular tachycardia. Arrhythmia was defined by the occurrence of ICD therapy (e.g.: antitachycardia pacing therapy, cardioversion or defibrillation).

	Definite ARVC (N = 18)	Borderline ARVC (N = 5)	Other arrhythmias (N = 12)	P
Sex				.61
Male	13 (72%)	4 (80%)	7 (58%)	
Female	5 (28%)	1 (20%)	5 (42%)	
Age at ^{123}I-MIBG (years)	45 (± 15)	64 (± 8.6)	43 (± 15)	.98
Age at initial diagnose (years)	39 (± 14)	58 (± 7.9)	37 (± 17)	.99
Weight (kg)	80 (± 11)	86 (± 6)	81 (± 21)	.78
Height (cm)	180 (± 6.4)	170 (± 5.6)	180 (± 9.6)	.39
Administered dose of ^{123}I-MIBG (MBq)	360 (± 46)	360 (± 15)	360 (± 44)	.94
Symptoms	8 (44%)	1 (20%)	0	.07
ICD	16 (89%)	2 (40%)	11 (92%)	.04
Arrhythmia before ^{123}I-MIBG	12 (67%)	1 (20%)	11 (92%)	.01
Arrhythmia within 4 years after ^{123}I-MIBG	7 (39%)	1 (20%)	1 (8%)	.13
CPR before ^{123}I-MIBG	5 (28%)	1 (20%)	11 (92%)	<.01
CVRF	13 (72%)	5 (100%)	7 (58%)	.54

^{123}I-MIBG, ^{123}Iodo-Metaiodbenzylguanidin; *CPR*, cardiopulmonary resuscitation; *CVRF*, cardiovascular risk factors; *ICD*, implantable cardioverter defibrillator.

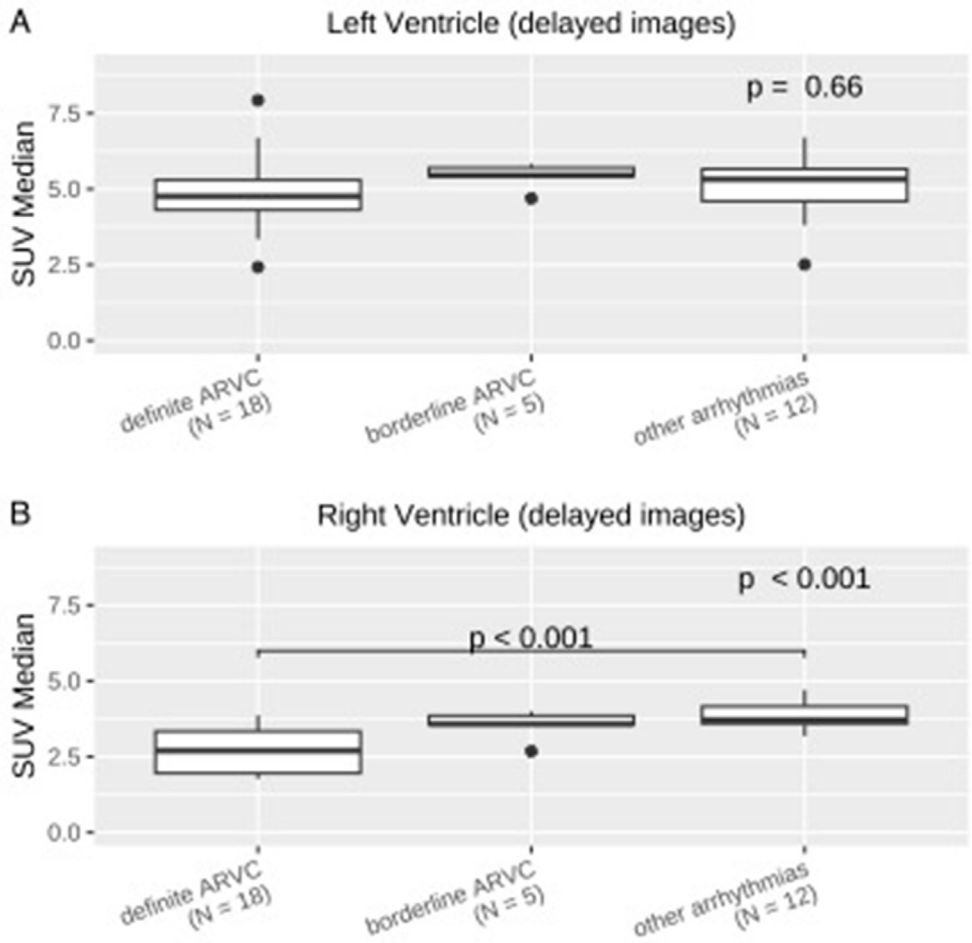

Figure 3. The SUV in delayed images was differentiated according to left (A) and right (B) ventricel in patients with various cardiac diseases, as depicted in boxplots. LV-SUVs are not significantly different. In contrast, RV-SUVs show a significant different between patients with definite ARVC and those with other arrhythmias. ANOVA and t-test were used.

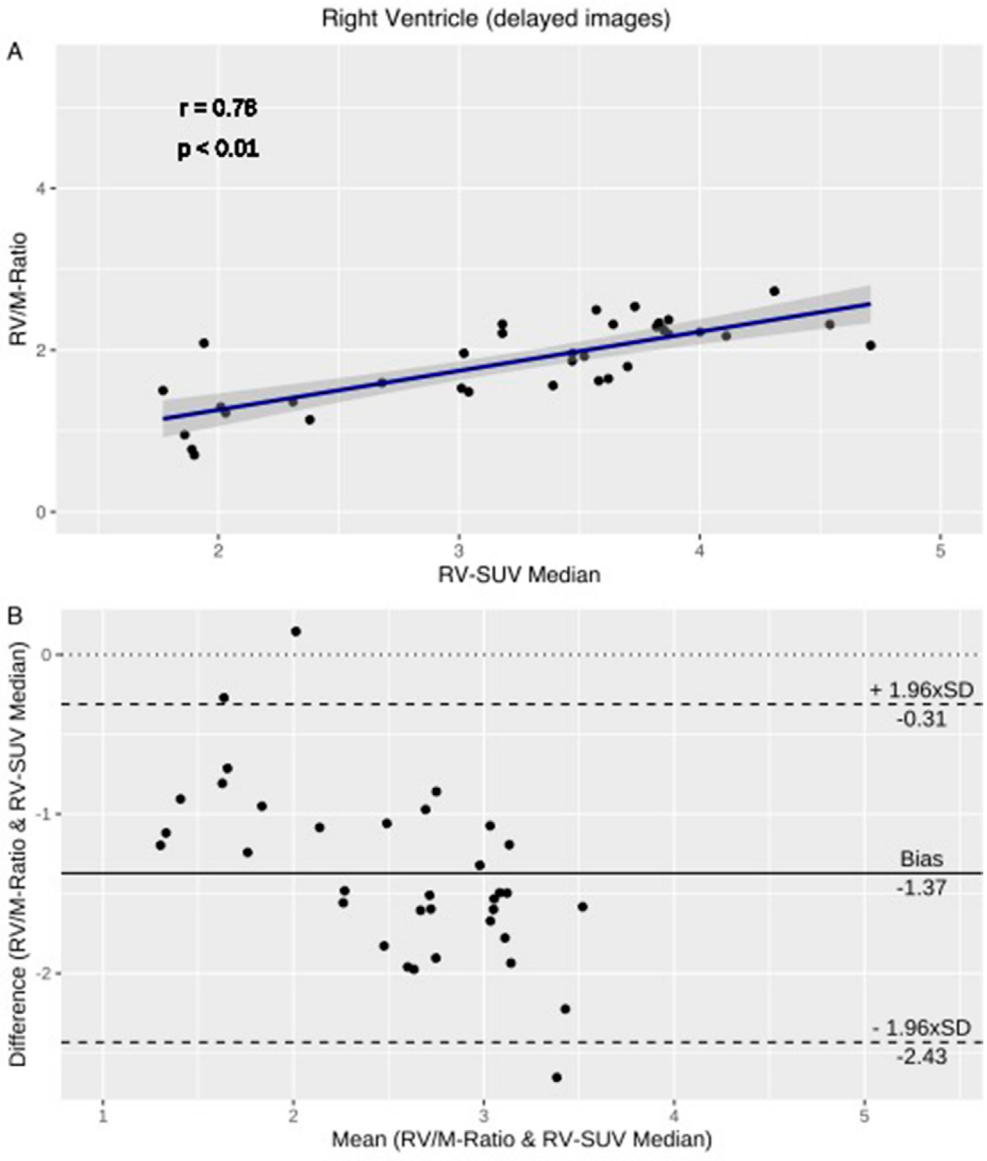

Figure 4. (A) Correlation between RV-SUV and RV/M-Ratio. (B) Bland-Altman-Plot as a comparison between the RV/M-Ratio and RV-SUV. Evaluation of delayed images. (A) The Pearson correlation coefficient and Pearsons's test were used. (B) A Bland Altman calculation and plot were performed.

this purpose, we assessed cardiac ^{123}I-MIBG images of patients with definite ARVC, borderline ARVC, and other arrhythmias and compared these images with echocardiographic parameters. This is the first study to analyze ^{123}I-MIBG absolute quantification in the LV and RV, which is feasible and correlates accurately with the gold standard H/M-Ratio. AUC comparing sensitivity and specificity favors RV-SUV to RV/M-Ratio for diagnosing ARVC. Reduced RV function was accompanied by lower ^{123}I-MIBG SUV in definite ARVC patients. Additionally, we provide insight into the utility of RV polar maps, showing globally reduced ^{123}I-MIBG uptake, but not RV segment-specific SUV reduction.

The quantitative evaluation of the scintigraphy data was feasible in all patients. The comparison between SUV and H/M-Ratio showed a significant correlation. The Bland-Altman-Plots demonstrated an agreement between both measurements. Considering the Biases, the SUV measured higher values than the H/M-Ratio across the study.

Previous studies have shown that patients suffering from ARVC exhibit sympathetic dysfunction, which can be analyzed with a lower

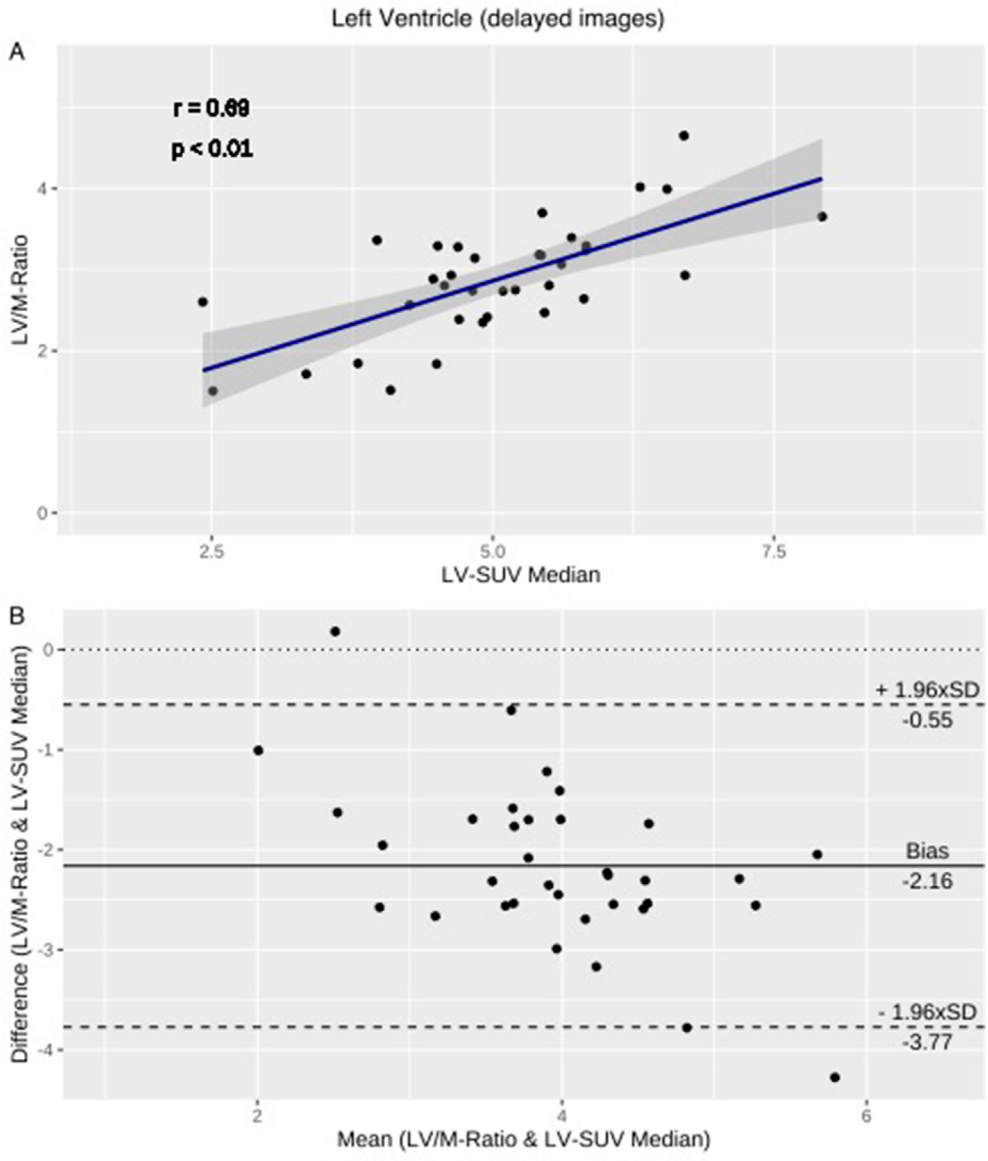

Figure 5. (A) Correlation between LV-SUV and LV/M-Ratio. (B) Bland-Altman-Plot as a comparison between the LV/M-Ratio and LV-SUV. Evaluation of delayed images. (A) The Pearson correlation coefficient and Pearsons's test were used. (B) A Bland Altman calculation and plot were performed.

accumulation of ^{123}I-MIBG as indicated by H/M-Ratio [17,33]. It was demonstrated that the RV in particular, is apparent with lower ^{123}I-MIBG H/M-Ratio in ARVC-patients [18,34]. In our study, we demonstrate that definite ARVC patients show a lower SUV in the RV compared to other groups. This difference was particularly evident between the definite ARVC group and the other arrhythmias group. Interestingly, the LV-SUV showed no significant difference between the groups in contrast to other studies [17,18].

Furthermore, the RV-SUV in delayed images appears to be suitable to distinguish between definite ARVC and other arrhythmias. The best discrimination could be achieved by using the RV-SUV, which aligns with a previous study [18]. However, no obvious advantage was demonstrated for the delayed images.

Burri et al. [35] reported no correlation between ^{123}I-MIBG uptake and LV-EF. In the present study, a significant correlation was observed between LV-SUV and LV-EF in early images, whereas in delayed images, the correlation was not significant. Moreover, the correlations between SUV and the FAC, a functional parameter for the RV, and between SUV and TAPSE were significant in both early and delayed images.

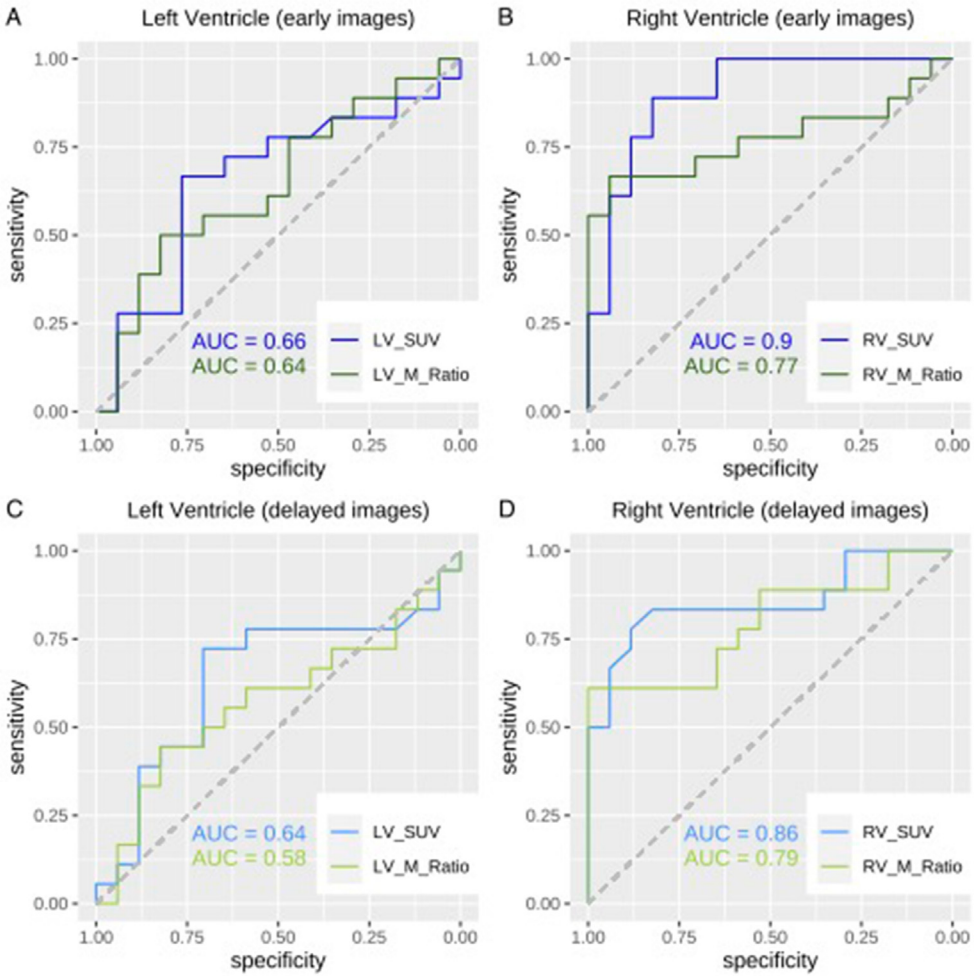

Figure 6. ROC and AUC for the LV and RV for early and delayed images. (A) Optimal cut-off value for the LV in early images: 6.81 (76.5% sensitivity, 66.7% specificity). (B) Optimal cut-off value for the RV in early images: 4.43 (82.4% sensitivity, 88.9% specificity). (C) Optimal cut-off value for the LV in delayed images: 5.09 (70.6% sensitivity, 72.2% specificity). (D) Optimal cut-off value for the RV in delayed images: 3.47 (88.2% sensitivity, 77.8% specificity). ROC and AUC were calculated.

Table 2. **Echocardiographic data of the study population. Other arrhythmias includes idiopathic ventricular fibrillation (IVFib), long-QT-Syndrom, catecholaminergic polymorphic ventricular tachycardia, neurocardiogenic syncope, Torsade-de-pointes-tachycardia, ventricular tachycardia.**

	Definite ARVC (N = 16)	Borderline ARVC (N = 4)	Other arrhythmias (N = 9)	*P*
LV ED (cm)	4.6 (± .49)	4.7 (± .76)	4.7 (± .83)	.87
LV ES (cm)	3.8 (± .51)	3.7 (± .35)	3.1 (± .85)	.24
LV EDV (mL)	120 (± 40)	140 (± 33)	140 (± 36)	.20
LV ESV (mL)	61 (± 28)	55 (± 17)	64 (± 14)	.86
LV EF (%)	51 (± 10)	60 (± 9.2)	55 (± 12)	.40
RVOT PLAX (cm)	3.7 (± .85)	3.1 (± .38)	2.6 (± .71)	<.01
RVOT PSAX (cm)	3.1 (± .83)	2.9 (.06)	2.1 (.35)	.05
RV Base (cm)	4.6 (± 1.2)	3.5 (± .25)	3.6 (± .96)	.02
RV Mid (cm)	3.6 (± 1.0)	2.6 (± .40)	2.5 (± .67)	<.01
RV Length (cm)	7.2 (± .87)	7.3 (± .24)	6.9 (± 1.0)	.49
RV EDA (cm^2)	32 (± 10)	21 (± 4.3)	22 (± 6.9)	.01
RV ESA (cm^2)	24 (± 11)	12 (± 2.2)	13 (± 5.5)	<.01
FAC (%)	27 (± 11)	43 (± 4.8)	45 (± 9.9)	<.01
TAPSE (cm)	1.8 (± .54)	2.4 (± .46)	2.4 (± .15)	<.01

FAC, fractional area change; *IVF*, Idiopathic ventricular fibrillation; *LV ED*, LV diastolic dimension; *LV EDV*, LV end-diastolic volume; *LV EF*, LV ejection fraction; *LV ES*, LV systolic dimension; *LV ESV*, LV end-systolic volume; *RV Base*, RV basal diameter; *RV EDA*, RV end-diastolic area; *RV ESA*, RV end-systolic area; *RV Length*, RV longitudinal diameter; *RV Mid*, RV mid-diameter; *RVOT PLAX*, RV outflow diameter in parasternal long-axis; *RVOT PSAX*, RV outflow diameter in parasternal short-axis; *TAPSE*, tricuspid annular plane systolic excursion. Values indicate Mean and SD.

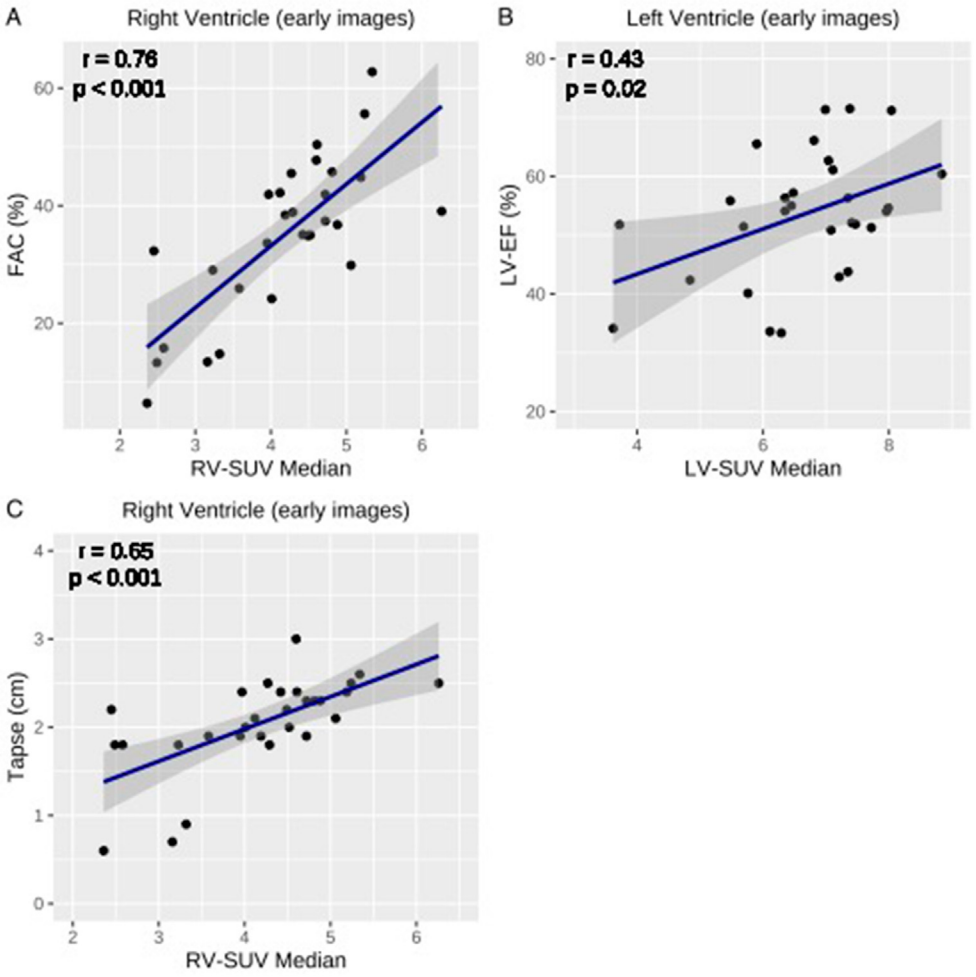

Figure 7. (A) Correlation of fractional area change (FAC) and RV-SUV. (B) Correlation of left ventricular ejection fraction (LV-EF) and LV-SUV. (C) Correlation of tricuspid annular plane systolic excursion (TAPSE) and RV-SUV. Evaluation of early images. The Pearson correlation coefficient and Pearsons's test were used.

Additionally, regional dysinnervation within the heart, which is considered prognostically relevant, could be examined by SPECT [36–38]. Various studies have demonstrated that a regional examination of the right ventricle is feasible for evaluating the perfusion [30,39]. Eguchi et al. [40] utilized RV polar map in ARVC patients to detect myocardial damage. Wichter et al. [17] identified regional abnormalities of sympathetic innervation as a cause of arrhythmia in patients suffering from ARVC. Our study shows that it was feasible to create a polar map of both the left and of the right ventricles in ^{123}I-MIBG scintigraphy to examinate regional differences. There was no segment with a significant difference evident in the RV, which may depend on the later stage of the disease. It is possible that early-diagnosed ARVC patients could exhibit regional but not global dysinnervation. In the LV, a few segments showed significant differences, primarily in the early images. If data for normal SUV values were available, similar to those for the H/M-Ratio [41], better discrimination of regions with divergent uptake might be possible.

Future prospective imaging studies are needed to evaluate the potential of SUV measurement to assess prognosis in ARVC patients regarding arrhythmia risk estimation.

A limitation of this study is the absence of SUV data in healthy hearts. This is particularly relevant considering Schäfers et al. [42] showed that patients with idiopathic ventricular fibrillation also exhibit reduced ^{123}I-MIBG values. The lack of healthy reference also limits the segmental uptake analysis. However, we aim to demonstrate that there is a global reduction in innervation rather than a specific pattern. Another limitation of this study is that ARVC is

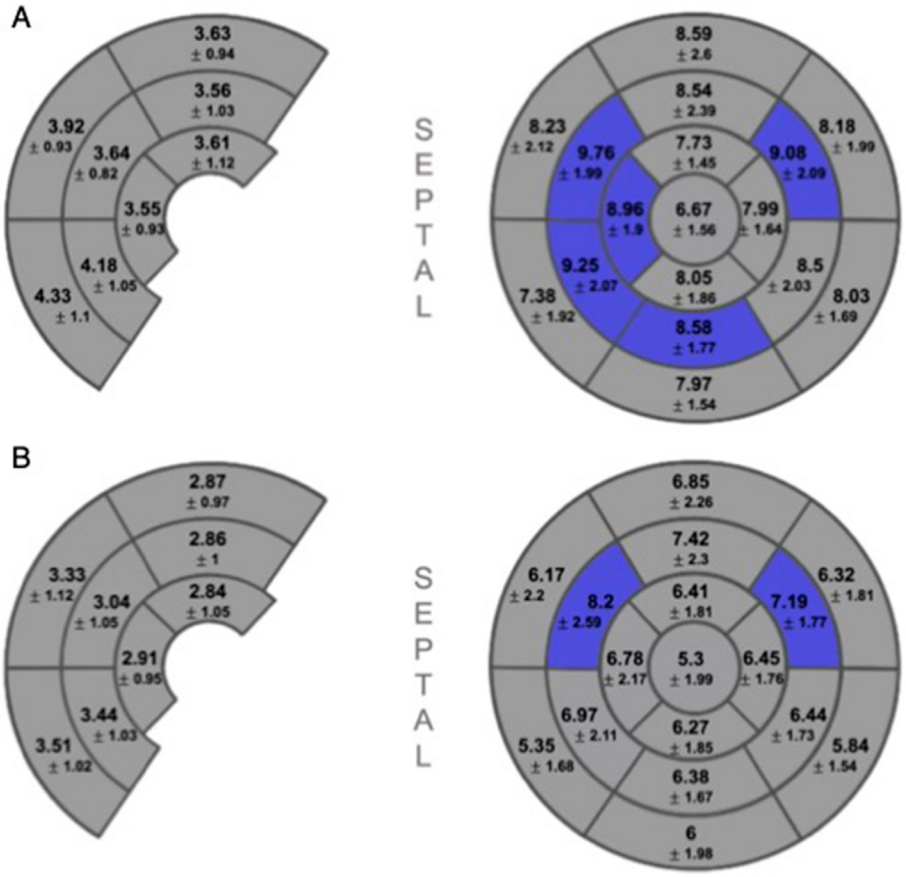

Figure 8. (A) Mean and standard deviation of the individual segments in early images, with the RV on the left side and the LV on the right sight. (B) Mean and standard deviation of the individual segments in delayed images, with the RV on the left side and the LV on the right sight. Data from patients diagnosed with definite ARVC were exclusively examined. Segments highlighted in blue indicate a significant difference from the mean of median LV-SUVs in the definite ARVC group. The *t*-test with Bonferroni adjustment was used.

a rare disease and subjects might be in different stages of the disease. Additionally, the ARVC cohort size included in our analysis might affect ROV curve statistics regarding early and delayed images. Furthermore, we cannot exclude the potential limitation of partial volume effect in this study. Due to the retrospective character of our study, we could not retrieve all echocardiographic parameters.

CONCLUSION

SUV analysis of ^{123}I-MIBG imaging could provide novel insights into the diagnosis and disease surveillance of ARVC patients. Our investigations may help to improve discrimination of ARVC patients from others suffering from arrhythmias. Our approach appears to be robust and suitable for clinical reporting, offering an advantage over the H/M-Ratio. Quantitative ^{123}I-MIBG SPECT in definite ARVC patients correlates well with RV function. Therefore, cardiac ^{123}I-MIBG imaging, using SUV and segmental RV analysis could enable image-guided surveillance and therapy in patients with ARVC.

NEW KNOWLEDGE GAINED

To our knowledge, this is the first study to determine quantitative cardiac ^{123}I-MIBG SPECT separately in the LV and RV in ARVC patients. The absolute quantification demonstrates a significant correlation with the gold standard H/M-Ratio. RV-SUV appears to be capable of distinguishing between patients suffering from ARVC and those with other arrhythmias. Furthermore, RV-SUV shows a significant correlation with functional echocardiographic parameters.

CLINICAL PERSPECTIVE

Quantitative cardiac ^{123}I-MIBG SPECT/CT is technically feasible for image-guided surveillance of ARVC patients.

RV-SUV values correlate well with functional echocardiographic parameters.

The separate assessment of the left and right ventricle offers a promising novel diagnostic opportunity to move from the current clinical standard of H/M-Ratio to absolute quantification of ^{123}I-MIBG SPECT/CT imaging.

FUNDING AND SUPPORT

M.B. was funded by the Deutsche Forschungsgemeinschaft (DFG, German Research Foundation) under Germany's Excellence Strategy within the framework of the Munich Cluster for Systems Neurology (EXC 2145 SyNergy; 390857198).

DISCLOSURES

The authors declare the following financial interests/personal relationships which may be considered as potential competing interests: Matthias Brendel reports a relationship with German Research Foundation that includes: funding grants. If there are other authors, they declare that they have no known competing financial interests or personal relationships that could have appeared to influence the work reported in this paper.

DATA AVAILABILITY STATEMENT

Raw data are available and can be retrieved upon a reasonable request to the corresponding author.

ACKNOWLEDGMENTS

None.

ETHICS APPROVAL

For this project, consent of the local ethics committee has been obtained (project number: 22-0328).

APPENDIX A. SUPPLEMENTARY DATA

Supplementary data to this article can be found online at https://doi.org/10.1016/j.nuclcard.2024.101911.

REFERENCES

[1] Maron BJ, Towbin JA, Thiene G, Antzelevitch C, Corrado D, Arnett D, et al. Contemporary definitions and classification of the cardiomyopathies: an American heart association scientific statement from the council on clinical cardiology, heart failure and transplantation committee; quality of care and outcomes research and functional genomics and translational biology interdisciplinary working groups; and council on epidemiology and prevention. Circulation 2006;113:1807–16.

[2] Corrado D, Basso C, Thiene G, McKenna WJ, Davies MJ, Fontaliran F, et al. Spectrum of clinicopathologic manifestations of arrhythmogenic right ventricular cardiomyopathy/dysplasia: a multicenter study. J Am Coll Cardiol 1997;30:1512–20.

[3] Corrado D, Link MS, Calkins H. Arrhythmogenic right ventricular cardiomyopathy. N Engl J Med 2017;376:61–72.

[4] te Riele AS, James CA, Groeneweg JA, Sawant AC, Kammers K, Murray B, et al. Approach to family screening in arrhythmogenic right ventricular dysplasia/cardiomyopathy. Eur Heart J 2016;37:755–63.

[5] Corrado D, Basso C, Judge DP. Arrhythmogenic cardiomyopathy. Circ Res 2017;121:784–802.

[6] Nava A, Bauce B, Basso C, Muriago M, Rampazzo A, Villanova C, et al. Clinical profile and long-term follow-up of 37 families with arrhythmogenic right ventricular cardiomyopathy. J Am Coll Cardiol 2000;36:2226–33.

[7] Lemola K, Brunckhorst C, Helfenstein U, Oechslin E, Jenni R, Duru F. Predictors of adverse outcome in patients with arrhythmogenic right ventricular dysplasia/cardiomyopathy: long term experience of a tertiary care centre. Heart 2005;91:1167–72.

[8] Rampazzo A, Nava A, Danieli GA, Buja G, Daliento L, Fasoli G, et al. The gene for arrhythmogenic right ventricular cardiomyopathy maps to chromosome 14q23-q24. Hum Mol Genet 1994;3:959–62.

[9] Sen-Chowdhry S, Syrris P, Ward D, Asimaki A, Sevdalis E, McKenna WJ. Clinical and genetic characterization of families with arrhythmogenic right ventricular dysplasia/cardiomyopathy provides novel insights into patterns of disease expression. Circulation 2007;115:1710–20.

[10] Christensen AH, Benn M, Bundgaard H, Tybjaerg-Hansen A, Haunso S, Svendsen JH. Wide spectrum of desmosomal mutations in Danish patients with arrhythmogenic right ventricular cardiomyopathy. J Med Genet 2010;47:736–44.

[11] Basso C, Thiene G, Corrado D, Angelini A, Nava A, Valente M. Arrhythmogenic right ventricular cardiomyopathy. Dysplasia, dystrophy, or myocarditis? Circulation 1996;94:983–91.

[12] Xu T, Yang Z, Vatta M, Rampazzo A, Beffagna G, Pilichou K, et al. Compound and digenic heterozygosity contributes to arrhythmogenic right ventricular cardiomyopathy. J Am Coll Cardiol 2010;55:587–97.

[13] Leclercq JF, Coumel P. Characteristics, prognosis and treatment of the ventricular arrhythmias of right ventricular dysplasia. Eur Heart J 1989;10:61–7.

[14] Lemery R, Brugada P, Janssen J, Cheriex E, Dugernier T, Wellens HJ. Nonischemic sustained ventricular tachycardia: clinical outcome in 12 patients with arrhythmogenic right ventricular dysplasia. J Am Coll Cardiol 1989;14:96–105.

[15] Nava A, Canciani B, Daliento L, Miraglia G, Buja G, Fasoli G, et al. Juvenile sudden death and effort ventricular tachycardias in a family with right ventricular cardiomyopathy. Int J Cardiol 1988;21:111–26.

[16] Cerrone M, Marrón-Liñares GM, van Opbergen CJM, Costa S, Bourfiss M, Pérez-Hernández M, et al. Role of plakophilin-2 expression on exercise-related progression of arrhythmogenic right ventricular cardiomyopathy: a translational study. Eur Heart J 2022;43:1251–64.

[17] Wichter T, Hindricks G, Lerch H, Bartenstein P, Borggrefe M, Schober O, et al. Regional myocardial sympathetic dysinnervation in arrhythmogenic right ventricular cardiomyopathy. An analysis using 123I-meta-iodobenzylguanidine scintigraphy. Circulation 1994;89:667–83.

[18] Todica A, Siebermair J, Schiller J, Zacherl MJ, Fendler WP, Massberg S, et al. Assessment of right ventricular sympathetic dysfunction in patients with arrhythmogenic right ventricular cardiomyopathy: an (123)I-

metaiodobenzylguanidine SPECT/CT study. J Nucl Cardiol 2020;27:2402–9.
[19] Merlet P, Valette H, Dubois-Randé JL, Moyse D, Duboc D, Dove P, et al. Prognostic value of cardiac metaiodobenzylguanidine imaging in patients with heart failure. J Nucl Med 1992;33:471–7.
[20] Merlet P, Benvenuti C, Moyse D, Pouillart F, Dubois-Randé JL, Duval AM, et al. Prognostic value of MIBG imaging in idiopathic dilated cardiomyopathy. J Nucl Med 1999;40:917–23.
[21] Agostini D, Verberne HJ, Burchert W, Knuuti J, Povinec P, Sambuceti G, et al. I-123-mIBG myocardial imaging for assessment of risk for a major cardiac event in heart failure patients: insights from a retrospective European multicenter study. Eur J Nucl Med Mol Imaging 2008;35:535–46.
[22] Lucignani G, Paganelli G, Bombardieri E. The use of standardized uptake values for assessing FDG uptake with PET in oncology: a clinical perspective. Nucl Med Commun 2004;25:651–6.
[23] Bailey DL, Willowson KP. An evidence-based review of quantitative SPECT imaging and potential clinical applications. J Nucl Med 2013;54:83–9.
[24] Dong F, Li L, Bian Y, Li G, Han X, Li M, et al. Standardized uptake value using thyroid quantitative SPECT/CT for the diagnosis and evaluation of graves' disease: a prospective multicenter study. BioMed Res Int 2019;2019:7589853.
[25] Kuji I, Yamane T, Seto A, Yasumizu Y, Shirotake S, Oyama M. Skeletal standardized uptake values obtained by quantitative SPECT/CT as an osteoblastic biomarker for the discrimination of active bone metastasis in prostate cancer. Eur J Hybrid Imaging 2017;1:2.
[26] Tabotta F, Jreige M, Schaefer N, Becce F, Prior JO, Nicod Lalonde M. Quantitative bone SPECT/CT: high specificity for identification of prostate cancer bone metastases. BMC Musculoskelet Disord 2019;20:619.
[27] Motegi K, Matsutomo N, Yamamoto T, Koizumi M. Evaluation of bone metastasis burden as an imaging biomarker by quantitative single-photon emission computed tomography/computed tomography for assessing prostate cancer with bone metastasis: a phantom and clinical study. Radiol Phys Technol 2020;13:219–29.
[28] Sato T, Matsutomo N, Yamamoto T, Fukami M, Kono T. Evaluation of standardized uptake value on 131I-6β-iodomethyl-19-norcholesterol scintigraphy for diagnosis of primary aldosteronism and correspondence with adrenal venous sampling. Ann Nucl Med 2023;37:89–98.
[29] Cerqueira MD, Weissman NJ, Dilsizian V, Jacobs AK, Kaul S, Laskey WK, et al. Standardized myocardial segmentation and nomenclature for tomographic imaging of the heart. A statement for healthcare professionals from the Cardiac Imaging Committee of the Council on Clinical Cardiology of the American Heart Association. Circulation 2002;105:539–42.
[30] Gimelli A, Pugliese NR, Bertasi M, Airò E, Bauleo C, Formichi B, et al. Cardio-pulmonary involvement in pulmonary arterial hypertension: a perfusion and innervation scintigraphic evaluation. J Nucl Cardiol 2021;28:546–56.
[31] Marcus FI, McKenna WJ, Sherrill D, Basso C, Bauce B, Bluemke DA, et al. Diagnosis of arrhythmogenic right ventricular cardiomyopathy/dysplasia: proposed modification of the task force criteria. Circulation 2010;121:1533–41.
[32] Lang RM, Badano LP, Mor-Avi V, Afilalo J, Armstrong A, Ernande L, et al. Recommendations for cardiac chamber quantification by echocardiography in adults: an update from the American Society of Echocardiography and the European Association of Cardiovascular Imaging. J Am Soc Echocardiogr 2015;28:1–39.e14.
[33] Lerch H, Bartenstein P, Wichter T, Hindricks G, Borggrefe M, Breithardt G, et al. Sympathetic innervation of the left ventricle is impaired in arrhythmogenic right ventricular disease. Eur J Nucl Med 1993;20:207–12.
[34] Siebermair J, Lehner S, Sattler SM, Rizas KD, Beckmann BM, Becker A, et al. Left-ventricular innervation assessed by (123)I-SPECT/CT is associated with cardiac events in inherited arrhythmia syndromes. Int J Cardiol 2020;312:129–35.
[35] Burri H, Sunthorn H, Somsen A, Fleury E, Stettler C, Shah D, et al. Improvement in cardiac sympathetic nerve activity in responders to resynchronization therapy. Europace 2008;10:374–8.
[36] Boogers MJ, Borleffs CJ, Henneman MM, van Bommel RJ, van Ramshorst J, Boersma E, et al. Cardiac sympathetic denervation assessed with 123-iodine metaiodobenzylguanidine imaging predicts ventricular arrhythmias in implantable cardioverter-defibrillator patients. J Am Coll Cardiol 2010;55:2769–77.
[37] Bax JJ, Kraft O, Buxton AE, Fjeld JG, Parízek P, Agostini D, et al. 123 I-mIBG scintigraphy to predict inducibility of ventricular arrhythmias on cardiac electrophysiology testing: a prospective multicenter pilot study. Circ Cardiovasc Imaging 2008;1:131–40.
[38] Clements IP, Kelkar AA, Garcia EV, Butler J, Chen J, Folks R, et al. Prognostic significance of (123)I-mIBG SPECT myocardial imaging in heart failure: differences between patients with ischaemic and non-ischaemic heart failure. Eur Heart J Cardiovasc Imaging 2016;17:384–90.
[39] Chiba J, Takeishi Y, Abe S, Tomoike H. Visualisation of exercise-induced ischaemia of the right ventricle by thallium-201 single photon emission computed tomography. Heart 1997;77:40–5.
[40] Eguchi M, Tsuchihashi K, Hashimoto A, Uno K, Kyuma M, Takahashi T, et al. Quantitative assessment of right ventricular structural abnormalities by right ventricular polar mapping of single photon emission computed tomogram. Nucl Med Commun 2002;23:943–50.
[41] Nakajima K. Normal values for nuclear cardiology: Japanese databases for myocardial perfusion, fatty acid and sympathetic imaging and left ventricular function. Ann Nucl Med 2010;24:125–35.
[42] Schäfers M, Wichter T, Lerch H, Matheja P, Kuwert T, Schäfers K, et al. Cardiac 123I-MIBG uptake in idiopathic ventricular tachycardia and fibrillation. J Nucl Med 1999;40:1–5.